

## Article

# Uniformly Dispersed Cu Nanoparticles over Mesoporous Silica as a Highly Selective and Recyclable Ethanol Dehydrogenation Catalyst

Yan Hao <sup>1,\*</sup> , Dajie Zhao <sup>1</sup>, Wen Liu <sup>1</sup>, Min Zhang <sup>2</sup>, Yixiao Lou <sup>1</sup>, Zhenzhen Wang <sup>1</sup>, Qinghu Tang <sup>1,\*</sup> and Jinghe Yang <sup>2,\*</sup> 

<sup>1</sup> Laboratory of Green Chemical Media and Reactions, School of Chemistry and Chemical Engineering, Collaborative Innovation Center of Henan Province for Green Manufacturing of Fine Chemicals, Key Ministry of Education, Henan Normal University, Xinxiang 453000, China

<sup>2</sup> School of Chemical Engineering, Zhengzhou University, Zhengzhou 450006, China

\* Correspondence: yanhao@htu.edu.cn (Y.H.); tangqinghu@htu.edu.cn (Q.T.); jhyang@zzu.edu.cn (J.Y.)

**Abstract:** Selective dehydrogenation of ethanol to acetaldehyde has been considered as an important pathway to produce acetaldehyde due to the atom economy and easy separation of acetaldehyde and hydrogen. Copper catalysts have attracted much attention due to the high activity of Cu species in O-H and C-H bonds oxidative cleavage, and low process cost; however, the size of the Cu nanoparticle is difficult to control since it is easily suffers from metal sintering at high temperatures. In this work, the Cu/KIT-6 catalyst exhibited an ultra-high metal dispersion of 62.3% prepared by an electrostatic adsorption method, due to the advantages of the confinement effect of mesoporous nanostructures and the protective effect of ammonia water on Cu nanoparticles. The existence of an oxidation atmosphere had a significant effect on the valence state of copper species and enhancing moderate acid sites. The catalyst treated by reduction and then oxidation possessed a moderate/weak acid site ratio of ~0.42 and a suitable proportion of Cu<sup>+</sup>/Cu<sup>0</sup> ratio of ~0.53, which conceivably rendered its superior ethanol conversion of 96.8% and full acetaldehyde selectivity at 250 °C. The catalyst also maintained a high selectivity of >99% to acetaldehyde upon time-on-stream of 288 h.

**Keywords:** copper; ethanol dehydrogenation; mesoporous silica



**Citation:** Hao, Y.; Zhao, D.; Liu, W.; Zhang, M.; Lou, Y.; Wang, Z.; Tang, Q.; Yang, J. Uniformly Dispersed Cu Nanoparticles over Mesoporous Silica as a Highly Selective and Recyclable Ethanol Dehydrogenation Catalyst. *Catalysts* **2022**, *12*, 1049. <https://doi.org/10.3390/catal12091049>

Academic Editor: Lucjan Chmielarz

Received: 26 August 2022

Accepted: 10 September 2022

Published: 15 September 2022

**Publisher's Note:** MDPI stays neutral with regard to jurisdictional claims in published maps and institutional affiliations.



**Copyright:** © 2022 by the authors. Licensee MDPI, Basel, Switzerland. This article is an open access article distributed under the terms and conditions of the Creative Commons Attribution (CC BY) license (<https://creativecommons.org/licenses/by/4.0/>).

## 1. Introduction

Acetaldehyde is a valuable chemical, widely used as feedstock for the chemical production of acetic acid, ethyl acetate, acetic anhydride, pyridine, and other important chemicals. Acetaldehyde can be produced by many processes, such as partial oxidation of ethane, hydration of acetylene, oxidation of ethylene, oxidative dehydrogenation of ethanol, and dehydrogenation of ethanol [1]. The selective dehydrogenation of ethanol to acetaldehyde has been considered as an important pathway to produce acetaldehyde because of the atom economy, viability of the reaction, and easy separation of acetaldehyde and hydrogen, which meets the requirement of green chemistry [2]. Copper catalysts have shown great potential in the ethanol dehydrogenation reaction due to the high activity of Cu species in O-H and C-H bonds oxidative cleavage and low process cost [3], however, the size of the Cu nanoparticle is difficult to control since it easily suffers from metal sintering at high temperatures [2,4]. Hence, it is important to prepare uniformly dispersed Cu nanoparticles with high activity and acetaldehyde selectivity.

Good support has improved the dispersion of Cu nanoparticles on the catalyst, leading to an increase in catalytic activity and stability. Metal oxides have commonly been used as supports due to their abundant surface functional groups, good stability, and easy availability [5]. Supported copper catalysts, such as Cu/ZnO, Cu/Al<sub>2</sub>O<sub>3</sub>, Cu/SiO<sub>2</sub>, Cu/ZrO<sub>2</sub>, and Cu/Al<sub>2</sub>O<sub>3</sub>-ZrO<sub>2</sub>, have been developed for the dehydrogenation of alcohols.

Summarizing the reported literatures, the  $ZrO_2$  support strongly stabilized the metals, and Cu nanoparticles supported on am- and t- $ZrO_2$  had smaller nanocluster sizes (4.4 and 2.9 nm, respectively) than Cu/m- $ZrO_2$  (8.7 nm). However, the Cu/ $ZrO_2$  catalyst exhibited high selectivity to ethyl acetate due to the high oxygen mobility from the  $ZrO_2$  phase to copper species and Lewis acidic sites, which were involved in acetaldehyde chemisorption, thus, resulted in the improvement of ethyl acetate selectivity [6]. The Cu nanoparticles supported on ZnO and  $Al_2O_3$  materials also showed high catalytic activity of ethanol, but with low selectivity for acetaldehyde [7,8]. The participation of ZnO with low acidity benefited the conversion of acetaldehyde to ethyl acetate [9]. The Cu/ $Al_2O_3$  catalyst showed lower selectivity to acetaldehyde due to the high acidity favoring ethanol dehydration to ethylene [10,11]. Cu nanoparticles supported on  $SiO_2$  showed high selectivity to acetaldehyde formation due to the nearly neutral surface, avoiding side reactions such as ethanol dehydration, condensation or decomposition at elevated temperatures, by the presence of acid and base sites, which confirmed that the role of the Cu-support interface played a significant effect on the dehydrogenative reaction [11]. Comparatively, the  $SiO_2$  support possessed high specific surface area and excellent thermal stability, which offered abundant active sites for ethanol adsorption, facilitating the formation of the acetaldehyde species.

Ordered mesoporous silica has attracted much attention because it can significantly improve the adsorption and diffusion properties of reactants and facilitate the “size effect” of the dispersion of metal nanoparticles. Better dispersion of the active species will be favorable for enhancing the redox capability of metal oxides as well as their reactivity. It has been reported that some ordered mesoporous silica materials, for instance, SBA-15, KIT-6, HMS, and MCM-41, have been studied as supports because of their ordered pore channels and narrow pore size distribution, which are beneficial to the dispersion of active metal and accessibility of active sites [12]. Zhou’s group reported the preparation of a CuO/KIT-6 catalyst by the excess impregnation method with a particle size of 9.6 nm [13]. Gallo’s group reported the synthesis of copper supported on MCM-41 by a one-pot methodology [14]. A catalyst with 10 wt% Cu exhibited a small particle size (1.8 nm) and displayed an ethanol conversion of 90% and acetaldehyde selectivity of 90% at 300 °C. It was found that higher Cu loading could improve the overall conversion of ethanol, but selectivity to acetaldehyde formation significantly decreased. Cu/SBA-15 and Cu/MCM-41 catalysts prepared by incipient wetness impregnation with a wide size distribution of copper nanoparticles showed the acetaldehyde yield for Cu/SBA-15 and Cu/MCM-41 catalysts were 27% and 24% at 300 °C, respectively [15]. It has been demonstrated that a high metal dispersion could significantly shorten the distance between metal active sites and improve metal utilization efficiency [16]. Mesoporous-silica-supported Cu nanoparticles prepared by the traditional impregnation method commonly lacked particle size control and uniformity, mainly due to the formation of nanoparticles directly on the support [17]. Therefore, it is of great significance to find a new way to prepare supported Cu nanocatalysts with high dispersion.

It has been found that the introduction of ammonia water during the impregnation process seems to be a good method to prepare a high dispersion of Cu nanoparticles [18]. In this work, combined with the advantages of the confinement effect of mesoporous nanostructures and the protective effect of ammonia water on Cu nanoparticles, the Cu nanocatalysts supported on various mesoporous silica supports were prepared by electrostatic adsorption method based on copper ammonia solution as the precursor, which was formed from copper nitrate dissolved in an excess of aqueous ammonia water. The ethanol dehydrogenation reaction was carried out in a fixed-bed reactor with atmosphere pressure. Considering the interaction of Cu species with support, and the interaction of intermediate and product with support, this work selected the proper support by investigating the effect of various mesoporous structures on the size and dispersion of Cu nanoparticles and catalytic behaviors. Moreover, the thermal treatment atmosphere was further studied to explore the effect of Cu valences on catalytic activities. The recyclability and reaction mechanism were also investigated.

## 2. Results and Discussion

### 2.1. Synthesis of Uniformly Dispersed Cu Nanoparticles over Mesoporous Silica

Cu nanoparticles supported on mesoporous silica were prepared by electrostatic adsorption method, based on copper ammonia solution as the precursor. The pore structure of mesoporous silica was considered to be a significant factor affecting the distribution of metal nanoparticles and catalytic behaviors, due to the effective confinement of metal nanoparticles by a mesoporous structure. Thus, three mesoporous silica supports with different pore structures named as SBA-15, KIT-6 and HMS, were selected as supports to explore the support structure effect on metal dispersion and catalytic behaviors. The schematic illustration of the catalysts' synthesis is shown in Figure 1.

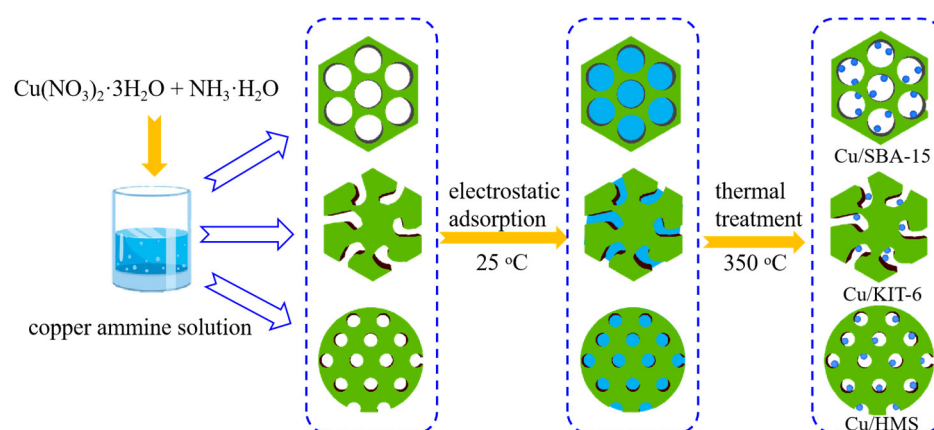


**Figure 1.** Schematic illustration for the synthesis of Cu/SBA-15, Cu/KIT-6, and Cu/HMS catalysts.

The  $N_2$  adsorption isotherms (Figure 2a) and pore size distributions (Figure 2b) of Cu/KIT-6, Cu/SBA-15, and Cu/HMS catalysts were determined by nitrogen adsorption analysis, and the textural parameters are shown in Table 1. The  $N_2$  adsorption isotherm of these catalysts all displayed type IV isotherm, proving mesoporous characteristics. The Cu/KIT-6 catalyst had an H1 type hysteresis loop ranging from 0.6 to 0.8, signifying typical mesoporous structures of uniform pore size. Well-defined and steep hysteresis loops indicated a narrow pore size distribution, which was consistent with the pore size distribution curves. While the adsorption hysteresis loop of Cu/SBA-15 was wider than that of Cu/KIT-6, a wider pore size distribution over Cu/SBA-15 was observed. The pore size distribution of SBA-15 was concentrated at  $\sim 7.17$  nm, Cu/KIT-6 was concentrated at  $\sim 4.74$  nm, while a narrow pore size distribution was concentrated around  $\sim 3.67$  nm for Cu/HMS. The wide-angle XRD patterns of the catalysts are displayed in Figure 2c. It was difficult to find the obvious diffraction peaks of  $CuO_x$  or Cu-related phase for all catalysts, which indicated that Cu nanoparticles might be uniformly dispersed over the support with small Cu nanoparticles [19]. The small-angle XRD patterns are given in Figure 2d. Cu/KIT-6 had an intense diffraction peak at  $2\theta \approx 0.95^\circ$  accompanied by two weak peaks at  $1.10^\circ$  and  $1.82^\circ$ , indexed as (211), (220), and (332) reflections, respectively, corresponding to the cubic three-dimensional pore structure [20]. The peaks at  $0.85^\circ$ ,  $1.48^\circ$ , and  $1.71^\circ$  corresponded to the characteristic peaks of the (100), (110), and (200) planes of SBA-15 with a hexagonal structure, which indicated the formation of ordered mesoporous structures [21]. The XRD pattern of the Cu-HMS featured the (100) diffraction peak accompanied by broader, unresolved higher order reflections, indicating that the catalyst also possessed a mesostructure [22]. In order to determine the effect of the support nanostructure after Cu deposition, the XRD spectra of HMS and Cu/HMS were obtained, as shown in Figure S1. The results showed that there were no obvious differences between the two samples, which indicated that the introduction of Cu nanoparticles into the supports did not interfere with the structural ordering of the supports.

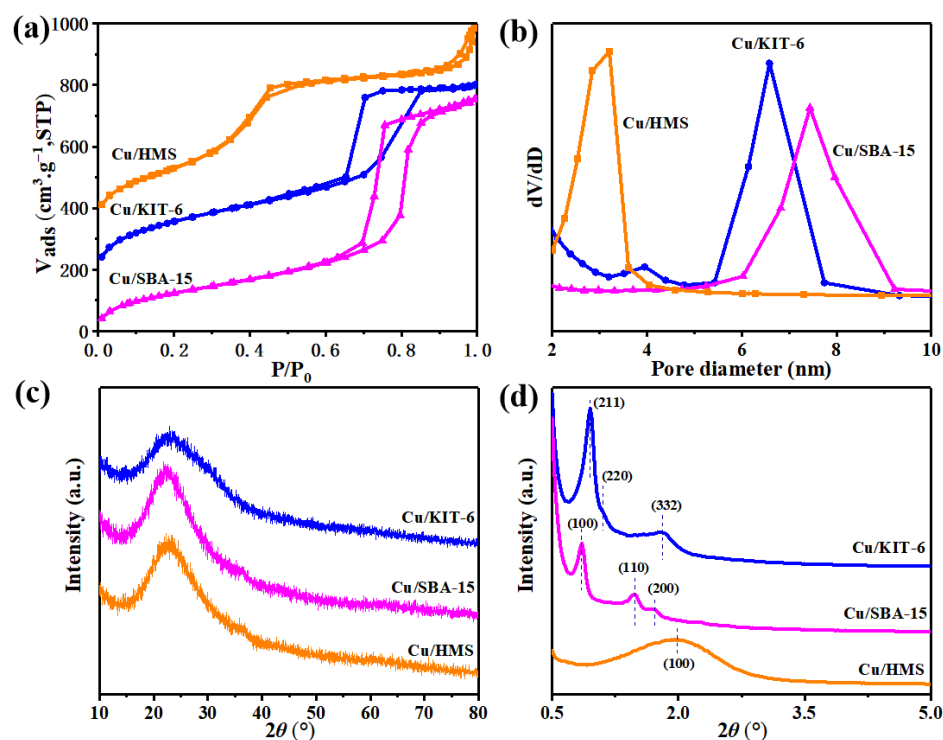


**Figure 2.** (a) Nitrogen adsorption isotherms, (b) pore size distributions, (c) wide-angle, and (d) small-angle XRD patterns, of Cu/KIT-6, Cu/SBA-15, and Cu/HMS catalysts.

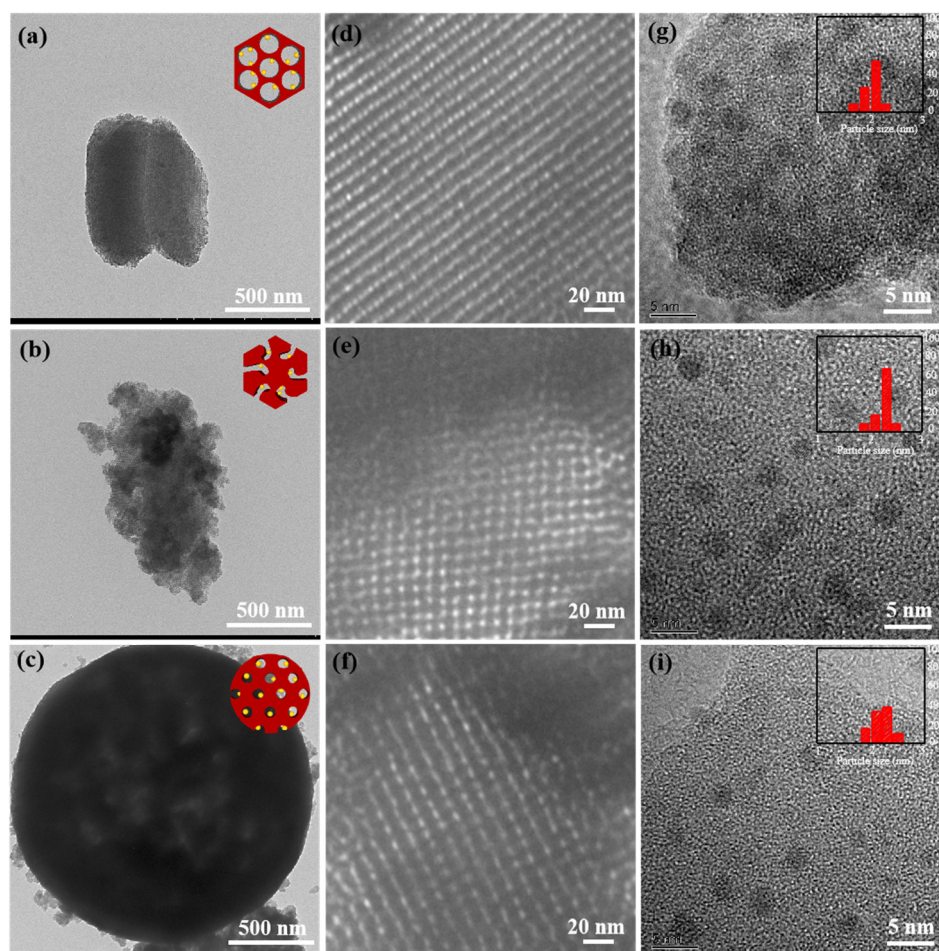
**Table 1.** The texture structure and catalytic activities of the investigated catalysts.

Catalysts	Size (nm)	Cu Dispersion (%) <sup>a</sup>	$S_{BET}$ (m <sup>2</sup> /g)	$V_{pore}$ (cm <sup>3</sup> /g)	$D_{pore}$ (nm)	Acidity (mmol NH <sub>3</sub> g <sup>-1</sup> ) <sup>b</sup>		$X_{ethanol}$ (%) <sup>c</sup>	$S_{acetaldehyde}$ (%) <sup>c</sup>
						Weak	Moderate		
Cu/KIT-6	2.01	62.3	920	1.25	4.74	0.122	0.051	96.8	99.8
Cu/SBA-15	2.24	60.9	640	1.12	7.17	0.122	0.048	92.8	96.8
Cu/HMS	2.21	60.2	918	1.07	3.67	0.126	0.037	89.4	94.5

<sup>a</sup> Cu dispersion was determined by the N<sub>2</sub>O titration method. <sup>b</sup> Acidity from NH<sub>3</sub>-TPD analysis of the sample. <sup>c</sup> Ethanol conversion and acetaldehyde selectivity of the investigated catalysts. Reaction condition: a reactant ethanol stream of 2 kPa balanced by N<sub>2</sub> under atmospheric pressure and WHSV of 13.67 mmol g<sup>-1</sup><sub>Cu</sub> h<sup>-1</sup>, 250 °C.

TEM images of the catalysts are shown in Figure 3, which explore the morphology and metal size of the catalysts. Cu/SBA-15 showed a well-defined worm-like morphology, and Cu/KIT-6 and Cu/HMS showed a typical rod-like and spherical morphology, respectively. Figure 3d revealed well-ordered 2D hexagonal arrays with uniform pore sizes of ~6.8 nm and parallel-arranged channels over the SBA-15 support. Figure 3e displayed an ordered cubic mesostructure with well-ordered cubic pores over the KIT-6 support. The mesoporous tubular channel with a mean size of ~3.7 nm over an HMS support could also be clearly observed. Remarkably, the Cu nanoparticles were uniformly dispersed with the spherical morphology over all the catalysts, as observed in Figure 3g–i. The mean nanoparticle sizes of the Cu/SBA-15, Cu/KIT-6 and Cu/HMS catalysts were ~2.24 nm, ~2.01 nm, and ~2.21 nm, respectively, by measurement of the metal diameter of at least 100 nanoparticles. Cu nanoparticles with high dispersion prepared by the electrostatic adsorption method can be analyzed from the following two aspects: the confinement effect of mesoporous nanostructures and the protective effect of ammonia water on Cu nanoparticles as a ligand. On the one hand, the Cu nanoparticles in all cases were smaller than their corresponding support inner pore sizes, and these nanoparticles were separately stabilized into the mesoporous channels, which confirmed that the mesoporous silica support effectively encapsulated the Cu nanoparticles. On the other hand, the cupric ammonium complex was adsorbed over

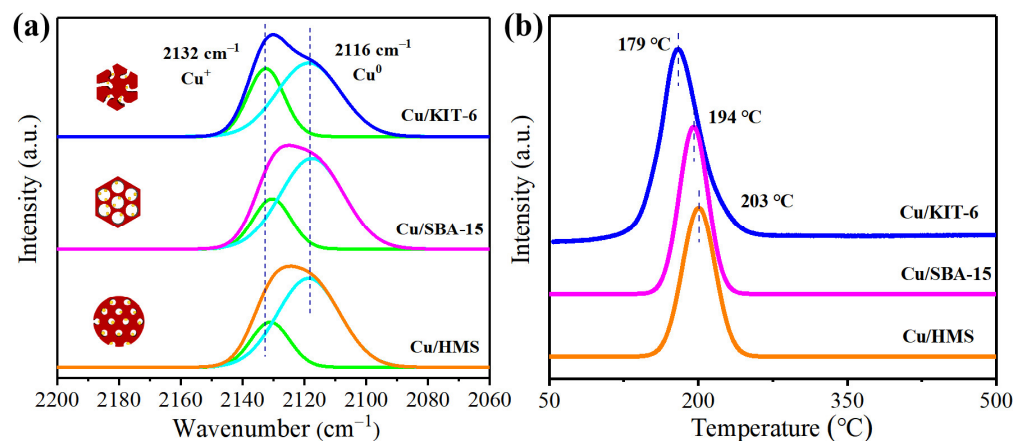
the silica surface under the action of electrostatic adsorption of anions and cations, and the strong interfacial interactions between Cu and mesoporous silica via Cu-O-Si bonds formed within a short time [23]. The highly dispersed Cu nanoparticles were successfully prepared based on the strong interfacial interaction between Cu and mesoporous silica via Cu-O-Si bonds, which inhibited the Cu nanoparticles aggregation [24]. The N<sub>2</sub>O titration results showed that the metal dispersion of Cu/SBA-15, Cu/KIT-6, and Cu/HMS catalysts were 60.9%, 62.3%, and 60.2%, respectively, which showed a higher metal dispersion compared with the reported literature [11,19,23]. The corresponding active surface area of Cu/SBA-15, Cu/KIT-6, and Cu/HMS catalysts were 30.6 m<sup>2</sup> g<sup>-1</sup><sub>cat.</sub>, 32.7 m<sup>2</sup> g<sup>-1</sup><sub>cat.</sub>, and 29.3 m<sup>2</sup> g<sup>-1</sup><sub>cat.</sub>, respectively. A high Cu dispersion and high active surface area are beneficial to achieving a good catalytic behavior in an ethanol dehydrogenation reaction.



**Figure 3.** TEM images and particle size distributions of Cu nanoparticles over Cu/SBA-15, Cu/KIT-6, and Cu/HMS catalysts. (a–c) The morphologies of the catalysts; (d–f) the pore sizes of the catalysts; (g–i) the Cu nanoparticle sizes of the catalysts.

CO-DRIFTS experiments were carried out to clarify the chemical state of the surface Cu species, and the spectroscopy is shown in Figure 4a. After CO adsorption, the spectra for the three catalysts displaying bands at  $\sim 2132$  cm<sup>-1</sup> and  $\sim 2115$  cm<sup>-1</sup> were assigned to the CO molecule adsorbed on Cu<sup>+</sup> ions and Cu<sup>0</sup> sites, respectively [25]. By integrating the curves, the Cu<sup>+</sup>/Cu<sup>0</sup> ratio of the Cu/KIT-6, Cu/SBA-15, and Cu/HMS catalysts, was  $\sim 0.53$ ,  $\sim 0.33$ , and  $\sim 0.31$ , respectively. It has been reported that the Cu<sup>+</sup>/Cu<sup>0</sup> mixture was the active site for ethanol dehydrogenation [26]. The results suggested that Cu/KIT-6 possessed a higher Cu<sup>+</sup>/Cu<sup>0</sup> active sites ratio, than the others. XPS analysis was also carried out to clarify the chemical state of the Cu species. As shown in Figure S2, the Cu 2p<sub>3/2</sub> and Cu 2p<sub>1/2</sub> peaks centered at binding energies of  $\sim 955$  eV, close to the broad satellite

peaks around  $\sim 943$  and  $\sim 963$  eV, was the characteristic peak for the highly dispersed  $\text{Cu}^{2+}$  species [27,28]. This was likely due to inadvertent exposure to air during sample storage. The Cu  $2p_{3/2}$  peaks of three samples centered at binding energies around  $\sim 933$  eV, were conventionally assigned to  $\text{Cu}^+$  or  $\text{Cu}^0$  species. The peak at 935 eV might be attributed to the  $\text{Cu}(\text{OH})_2$  phase, the formation of which may have been caused by the presence of ammonia water [29].



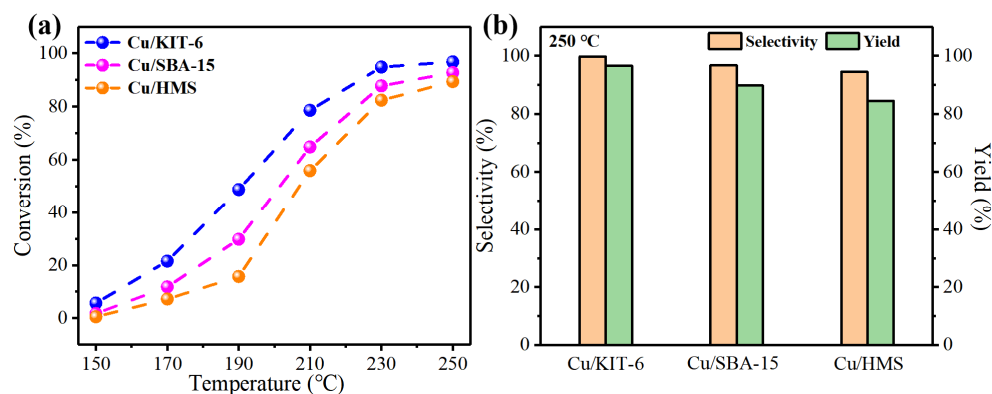
**Figure 4.** (a) In situ DRIFTS analysis of sequential adsorbed CO over Cu/KIT-6, Cu/SBA-15, and Cu/HMS catalysts; (b)  $\text{H}_2$ -TPR analysis of Cu/KIT-6, Cu/SBA-15, and Cu/HMS catalysts.

Figure 4b shows the  $\text{H}_2$ -TPR patterns of the catalysts, displaying their reduction behavior. The reduction peaks were located in the range of  $150$ – $250$  °C with the center peak around  $200$  °C. Li's group proposed that reduction peaks below  $350$  °C corresponded to the  $\text{Cu}^{2+}$  species reduced to  $\text{Cu}^+$  [30]. The  $\text{H}_2$  consumption peaks all exhibited a narrow and symmetrical temperature range, which indicated that the particle sizes of the active phase were uniformly dispersed. The results showed a typical reduction peak of  $\text{Cu}_2\text{O}$  at  $\sim 180$  °C for Cu/KIT-6, and the reduction peak at  $\sim 200$  °C for Cu/SBA-15 and Cu/HMS, which were ascribed to well-dispersed  $\text{CuO}_x$  nanoparticles. The lower reduction temperature of Cu/KIT-6, than Cu/SBA-15 or Cu/HMS, suggested the presence of finely dispersed smaller sized Cu nanoparticles with higher interaction with the silica support. Furthermore, the total  $\text{H}_2$  consumption amount of Cu/SBA-15, Cu/KIT-6, and Cu/HMS catalysts was calculated, as 905, 953, and 898  $\mu\text{mol/g}$ , respectively. Therefore, the  $\text{H}_2$  consumption amount of Cu/KIT-6 was larger than the other two catalysts due to the higher Cu dispersion and larger active surface area.

## 2.2. Catalytic Performances of Mesoporous-Silica-Supported Cu Nanoparticles

The catalytic performances of the prepared catalysts were evaluated with ethanol dehydrogenation reaction under atmospheric pressure, and the results are shown in Figure 5. A catalyst performance test of ethanol dehydrogenation was carried out in a fixed bed reactor under atmospheric pressure. Ethanol was fed to the system via a vaporizer, producing a reactant stream composed of ethanol (2 kPa) balanced by an  $\text{N}_2$  flow of 36 mL/min under atmospheric pressure, and WHSV (weight hourly space velocity) of  $13.67 \text{ mmol g}^{-1}_{\text{Cu}} \text{ h}^{-1}$ . Notably, the ethanol conversions of the catalysts increased with the reaction temperatures, due to the enhanced reaction rate as well as the nature of the endothermic reaction. The mesoporous silica with different pore-nanostructure-supported Cu nanocatalysts all exhibited excellent ethanol conversion ( $>89\%$ ) at  $250$  °C, attributed to the uniformly dispersed Cu nanoparticles. In addition, an almost complete conversion of ethanol over the three catalysts was observed above  $300$  °C. From the perspective of energy saving and environmental protection, we chose  $250$  °C as the reaction temperature for the following research and analysis. Among the three catalysts, Cu/KIT-6 showed a slightly higher conversion of 96.8% than Cu/SBA-15 (92.8%) or Cu/HMS (89.4%) at  $250$  °C. Combining the texture struc-

tures of Cu/KIT-6 and Cu/HMS, although the BET specific surface area of both samples was similar, the pore size distribution of Cu/KIT-6 (~4.74 nm) was slightly larger than of Cu/HMS (~3.67 nm). It was easier to achieve a high dispersion of Cu nanoparticles with the mesoporous silica with larger pores, which had a positive impact on the mass transfer of reactants and products, leading to good catalytic activity. Obviously, the catalytic activity of Cu/SBA-15 was better than Cu/HMS, which was attributed to the pore size distribution of Cu/SBA-15 (~7.17 nm) being significantly higher than that of Cu/HMS. This unique property of three-dimensional channel networks and ordered cubic mesostructure for the KIT-6 support provided highly opened spaces, by comparison with the SBA-15 with a linear channel structure, which could enhance the dispersion of Cu nanoparticles and faster diffusion of reactants and products during reaction, thus, possibly improving the reactivity [31]. The highest activity of Cu/KIT-6 was attributed to the presence of a three-dimensional mesopore structure and a large surface area, which implied a well-developed pore interconnectivity, the accessibility of the pore system, and benefitted the mass transfer from the reactant to the active sites. To confirm the support nanostructure effect on catalytic activities, we further calculated the reaction rate for the three catalysts at 250 °C, and the reaction rate decreased in the following order: Cu/KIT-6 ( $7.74 \text{ g}_{\text{EtOH}}/\text{g}_{\text{cat}}\cdot\text{s}$ ) > Cu/SBA-15 ( $7.24 \text{ g}_{\text{EtOH}}/\text{g}_{\text{cat}}\cdot\text{s}$ ) > Cu/HMS ( $7.15 \text{ g}_{\text{EtOH}}/\text{g}_{\text{cat}}\cdot\text{s}$ ). Moreover, the particle size, dispersion, and active surface area of Cu nanoparticles also played a key role in affecting the catalytic activity. Small Cu particles possessed a higher density of coordinatively unsaturated sites, e.g., corners and kinks, which were more reactive than steps or terrace sites [19]. A high Cu dispersion and high active surface area of Cu/KIT-6 were beneficial in achieving a good catalytic behavior in the ethanol dehydrogenation reaction, so that it exhibited a faster substrate reaction rate. Furthermore, the CO-DRIFT results also indicated that Cu/KIT-6 possessed a higher  $\text{Cu}^+/\text{Cu}^0$  active sites ratio than the other two catalysts; it has previously been reported that the  $\text{Cu}^+/\text{Cu}^0$  mixture is the active site for ethanol dehydrogenation [32].



**Figure 5.** (a) Ethanol conversion, and (b) acetaldehyde selectivity and yield, of Cu/KIT-6, Cu/SBA-15, and Cu/HMS catalysts. Reaction condition: a reactant ethanol stream of 2 kPa balanced by  $\text{N}_2$  under atmospheric pressure, and WHSV of  $13.67 \text{ mmol g}^{-1}_{\text{Cu}} \text{ h}^{-1}$ .

The acetaldehyde selectivity and yield of the catalysts are shown in Figure 5b. Acetaldehyde was the main product formed by the direct dehydrogenation of ethanol, and acetaldehyde could also be easily converted to other deep dehydrogenation by-products, such as ethylene, ethyl acetate, acetic acid, etc. The mesoporous silica with different pore-nanostructures-supported Cu nanocatalysts all exhibited excellent acetaldehyde selectivity, consistently exceeding 90.0%, due to the uniformly dispersed Cu nanoparticles. The Cu/KIT-6 catalyst exhibited a higher selectivity of acetaldehyde (99.8%) than Cu/SBA-15 (96.8%) or Cu/HMS (94.5%) at 250 °C. The differences were attributed to the quantities of exposed surface Si-OH groups and acid active sites over the surfaces of different silica supports. The three catalysts were further explored by in situ  $\text{NH}_3$ -FTIR and  $\text{NH}_3$ -TPD characterizations. The Cu/KIT-6 catalyst showed the band in the range of  $\sim 1558 \text{ cm}^{-1}$  commonly ascribed to adsorbed  $\text{NH}_3$  on Lewis acid sites and bands at  $\sim 1489 \text{ cm}^{-1}$  and

$\sim 1400\text{ cm}^{-1}$  assigned to adsorbed  $\text{NH}_4^+$  on Brönsted acid sites, as shown in Figure 6a. The results indicated that the Cu/KIT-6 catalyst possessed more abundant Lewis acid sites than Cu/SBA-15 and Cu/HMS, which may promote the selectivity of acetaldehyde [1]. Figure 6b showed that the curves of the three catalysts could be subdivided into three peaks, indicating the existence of at least two types of acid sites.  $\text{NH}_3$  species binding with Brönsted acid sites and Lewis acid sites have been well studied through in situ  $\text{NH}_3$ -FTIR analysis. The Brönsted acid site corresponding to the peak around  $\sim 103^\circ\text{C}$  was considered to be the catalytic active center formed by  $\text{NH}_4^+$  and  $\text{H}_2\text{O}$ , and the Lewis acid site corresponding to the peak at  $\sim 300^\circ\text{C}$  was considered to be the catalytic active center for  $\text{NH}_3$  adsorption and  $-\text{NH}_2$  formation [33]. In addition,  $\text{NH}_3$ -TPD results displayed that the Cu/KIT-6 catalyst exhibited a higher moderate/weak acid site ratio of  $\sim 0.42$  than Cu/SBA-15 ( $\sim 0.39$ ) and Cu/HMS ( $\sim 0.30$ ), which might have been caused by the different exposed surface Si-OH groups and specific mesostructure of the materials [34]. The total acidity of the three catalysts was in the order of Cu/KIT-6 > Cu/SBA-15 > Cu/HMS. It has been reported that weak acidic sites are responsible for a dehydration reaction, whereas dehydrogenation requires metallic and moderate acid sites [6]. The abundant amount of medium–strong acid sites over the KIT-6 support could lead to a higher acetaldehyde selectivity during the ethanol dehydrogenation process, which might be due to the more active centers that were generated. The acetaldehyde yield of 96.6% over the Cu/KIT-6 catalyst was also higher than Cu/SBA-15 (89.8%) or Cu/HMS (84.5%) at  $250^\circ\text{C}$ . As a result, the uniformly distributed Cu nanoparticles, the large active surface area and three-dimensional cubic pore structure, and the abundant acid sites, enabled this Cu/KIT-6 catalyst to behave as the best candidate in the ethanol dehydrogenation reaction.

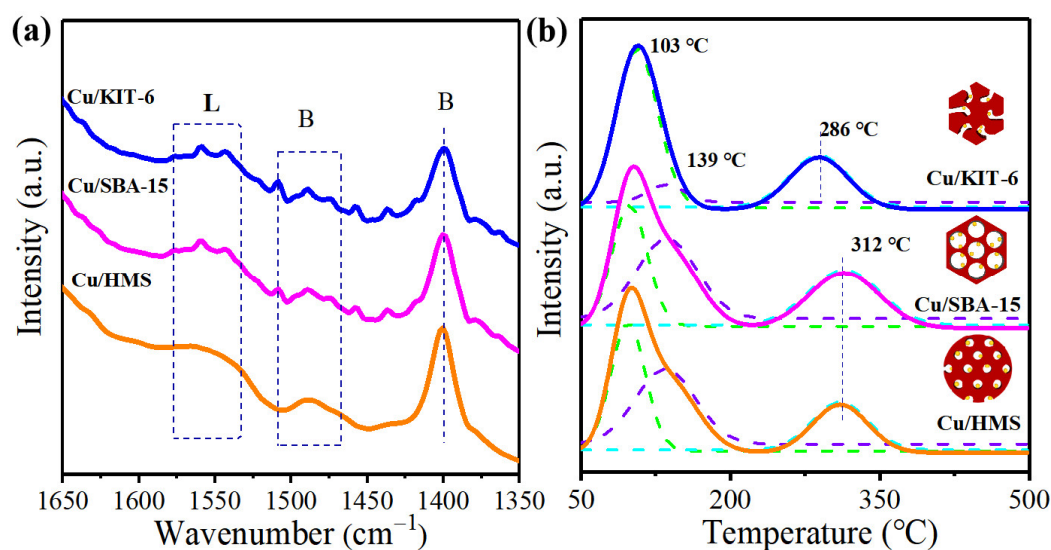


**Figure 6.** (a) In situ  $\text{NH}_3$ -FTIR spectra of Cu/KIT-6, Cu/SBA-15, and Cu/HMS catalysts at  $25^\circ\text{C}$ ; (b)  $\text{NH}_3$ -TPD analysis of Cu/KIT-6, Cu/SBA-15, and Cu/HMS catalysts.

To further explore the effect of ammonia water on catalytic behaviors, the Cu/KIT-6-none catalyst was prepared without  $\text{NH}_3 \cdot \text{H}_2\text{O}$  by the same preparation method. The TEM image of the Cu/KIT-6-none catalyst is shown in Figure S3a. In the absence of ammonia water as a ligand to protect the Cu nanoparticles from agglomeration, obviously aggregated Cu nanoparticles were formed. The conversion of Cu/KIT-6-none catalyst was only 6.46%, which decreased significantly compared with Cu/KIT-6 (conversion of 96.8%) at  $250^\circ\text{C}$ , as shown in Figure S3b. Therefore, based on the fact that ammonia water acted as a ligand to protect Cu nanoparticles from agglomeration, the results showed that Cu/KIT-6 exhibited excellent catalytic activity and high acetaldehyde yield, due to the uniformly dispersed Cu nanoparticles and the well-developed three-dimensional interconnected pore structures.

### 2.3. The Thermal Treatment Atmosphere Effect on Catalytic Behaviors

Based on the unique feature of ammonia water as a ligand to protect Cu nanoparticles from agglomeration, the Cu/KIT-6 catalyst with uniformly dispersed Cu nanoparticles and small particle size was successfully prepared by the electrostatic adsorption method. It has been verified from previous studies that the metal particle size and support pore structure of the catalyst significantly influences catalytic activity, and the charge of Cu species also plays a key factor in the ethanol dehydrogenation to acetaldehyde. Therefore, the effect of thermal treatment atmosphere on catalytic activities was further investigated based on KIT-6 as the support, and the treatment temperature was kept at 350 °C. In this part, the Cu/KIT-6 catalyst that was reduced under 10% H<sub>2</sub>/Ar atmosphere was named R, and the Cu/KIT-6 catalyst oxidized under 20% O<sub>2</sub>/N<sub>2</sub> atmosphere was named O. The catalyst was named RO, when it was reduced first, and then oxidized. The catalyst which was oxidized first, and then reduced, was named OR. The catalytic behaviors of these catalysts are shown in Table 2, and the activity of the catalysts treated with different atmospheres was significantly different. The results indicated that the highest conversion of 96.8% was obtained by the RO sample, which was slightly higher than R (94.5%) at 250 °C. To our disappointment, the catalytic activity of OR decreased to 40.4%, and even more seriously, the conversion of sample O was as low as 4.15%. Moreover, the acetaldehyde selectivity of these catalysts was also obviously distinct, and the selectivity of the catalysts was in the order of RO (99.8%) > O (89.9%) > R (81.4%) > OR (81.0%). The data clearly stated that the reducing or oxidative atmosphere had a significant effect on the catalytic activity of ethanol dehydrogenation.

**Table 2.** The texture structure of the Cu/KIT-6 catalyst under different treatment atmospheres.

Catalysts	Cu <sup>+</sup> /Cu <sup>0</sup> <sup>a</sup>	D <sub>(H<sub>2</sub>/Cu)</sub> <sup>b</sup>	Cu Nanoparticle Size (nm) <sup>c</sup>	Acidity (mmol NH <sub>3</sub> g <sup>-1</sup> ) <sup>d</sup>		X <sub>ethanol</sub> (%) <sup>e</sup>	S <sub>acetaldehyde</sub> (%) <sup>e</sup>
				Weak	Moderate		
RO	0.53	37.8%	2.01	0.122	0.051	96.8	99.8
R	0.21	1.8%	2.14	0.127	-	94.5	81.4
OR	-	0.7%	2.62	0.121	-	40.4	81.0
O	0.72	30.7%	4.00	0.126	0.102	4.10	89.9

<sup>a</sup> Cu<sup>+</sup>/Cu<sup>0</sup> ratio calculated from CO-DRIFTS analysis. <sup>b</sup> D<sub>(H<sub>2</sub>/Cu)</sub> refers to the reduced Cu content in the H<sub>2</sub>-TPR analysis. D<sub>(H<sub>2</sub>/Cu)</sub> = (B/A) × 100%, the peak areas of the CuO (Figure S4) and the Cu/KIT-6 are denoted as A and B, respectively. <sup>c</sup> Cu nanoparticle size calculated from XRD. <sup>d</sup> Acidity from NH<sub>3</sub>-TPD analysis of the sample. <sup>e</sup> Ethanol conversion and acetaldehyde selectivity of the Cu/KIT-6 catalyst under different pre-treatment atmospheres. Reaction condition: a reactant ethanol stream of 2 kPa balanced by N<sub>2</sub> under atmospheric pressure and WHSV of 13.67 mmol g<sup>-1</sup><sub>Cu</sub> h<sup>-1</sup>, 250 °C.

To further explore the reasons for the differences in catalytic behaviors, a series of characterization analyses were performed as follows. Figure 7a shows the XRD patterns of the samples, and no obvious diffraction peaks of metal or metal oxide nanoparticles were observed in the samples of RO, R, and OR, respectively, which indicated that the particles were small in size and uniformly distributed on the KIT-6 support, combined with previous TEM results. Distinctively, an obvious characteristic diffraction peak was found at 2θ ≈ 43.3° for sample O, which could be attributed to the CuO (111) lattice planes, identical to the compound given by calcination of the bulk nitrate trihydrate [35]. Due to the weak metal-support interaction and poor dispersion of CuO, which was not conducive to ethanol dehydrogenation, the O sample exhibited poor catalytic activity. Furthermore, an H<sub>2</sub>-TPR analysis was performed to clarify the presence of metal oxides and study the reducibility of copper species, which was carried out by in situ treatment under different atmospheres, as shown in Figure 7b. The active centers of the R and OR samples were almost metallic copper after reduction, and no obvious peaks were observed by H<sub>2</sub>-TPR. The RO sample exhibited a typical reduction peak at ~179 °C, which was related to the high dispersion and small size reduction of Cu<sub>2</sub>O in the literature [36]. The O sample directly treated in an oxidative atmosphere showed a strong peak at ~222 °C, which was attributed

to the presence of CuO [37], corresponding to the XRD results. The RO sample showed a slightly lower reduction temperature than O, due to the highly dispersed Cu nanoparticles being more easily reduced than the CuO particles. This result indicated that the RO sample was more easily exposed to the active site, which was favorable for ethanol conversion. CO-DRIFTS analysis was conducted to further explore the influence of the Cu charge on the catalytic activities of the RO, R, OR, and O samples via in situ treatment, and the corresponding spectra are shown in Figure 7c. After CO adsorption, the spectra displaying bands at  $\sim 2132\text{ cm}^{-1}$  and  $\sim 2115\text{ cm}^{-1}$  were assigned to the CO molecule adsorbed on  $\text{Cu}^+$  ions and  $\text{Cu}^0$  sites at a lower temperature, respectively. Importantly, it was observed from the spectrum of RO that both  $\text{Cu}^0$  and  $\text{Cu}^+$  sites existed on the metal surface after the metal was treated by reduction first and then oxidation. The existence of  $\text{Cu}^+$  was attributed to electron transfer from the Cu to the KIT-6 support as a result of strong interaction. The coexistence of  $\text{Cu}^+$  and  $\text{Cu}^0$  sites on the catalyst may account for the high activity of the RO sample [23]. A small amount of  $\text{Cu}^+$  ions appeared on the surface of R, indicating that a mixture of  $\text{Cu}^0$  sites and  $\text{Cu}^+$  ions could be obtained after direct reduction of the copper precursor. It was observed in the OR sample that  $\text{Cu}^+$  ions were almost completely converted to  $\text{Cu}^0$  sites after total oxidation and then reduction again. In the O sample after oxidization, both  $\text{Cu}^0$  and  $\text{Cu}^+$  sites existed. The  $\text{Cu}^+/\text{Cu}^0$  ratio of the RO and R samples were  $\sim 0.53$  and  $\sim 0.21$  at room temperature, separately (Table 2), which might account for the higher conversion of the RO sample (96.8%) than the R sample (94.5%). However, the O sample had a  $\text{Cu}^+/\text{Cu}^0$  ratio of  $\sim 0.72$  and its conversion was only 4.15%. The results showed that the conversion of ethanol was more favorable when the suitable proportion of  $\text{Cu}^+/\text{Cu}^0$  was  $\sim 0.53$ , which was consistent with previous reports [38]. In addition, the band of CO on  $\text{Cu}^0$  species gradually disappeared when the sample was degassed from  $50\text{ }^\circ\text{C}$  to  $75\text{ }^\circ\text{C}$ , while the band at  $\sim 2132\text{ cm}^{-1}$  for the RO sample became more evident compared with the other three catalysts at  $100\text{ }^\circ\text{C}$  (Figure 8). The migration of  $\text{Cu}^0$  to  $\text{Cu}^+$  also avoided the reduction of  $\text{Cu}^+$  to metallic Cu and enhanced the conversion in ethanol dehydrogenation, illustrating that the  $\text{Cu}^+$  species was responsible for the ethanol adsorbed and activated in this reaction [39]. Therefore, RO presented the highest conversion, due to the high metal dispersion and the suitable proportion of  $\text{Cu}^+/\text{Cu}^0$  ratio of  $\sim 0.53$ .

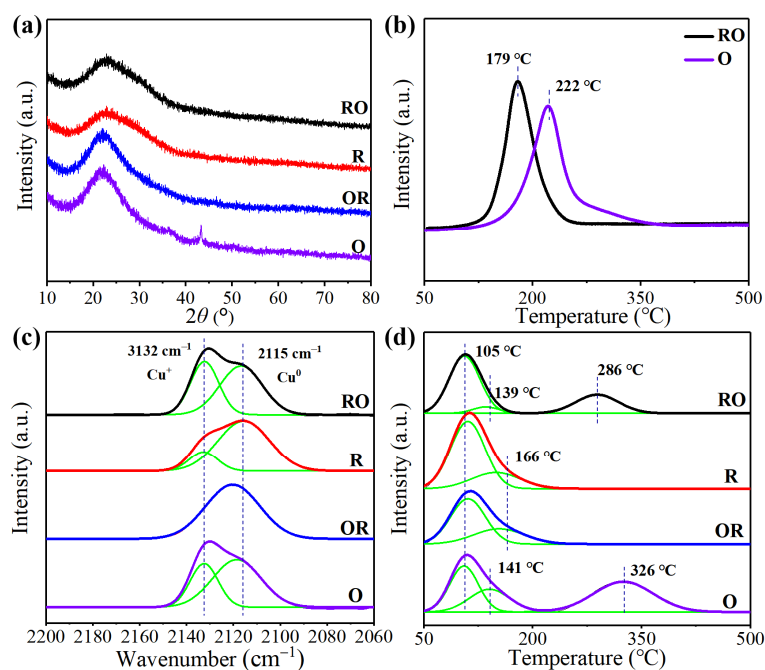


**Figure 7.** (a) Wide-angle XRD patterns, and (b)  $\text{H}_2$ -TPR analysis, of the Cu/KIT-6 catalyst under different treatment atmospheres. (c) In situ DRIFTS analysis of sequential adsorbed CO over the Cu/KIT-6 catalyst, and (d)  $\text{NH}_3$ -TPD analysis of the Cu/KIT-6 catalyst, under different treatment atmospheres.

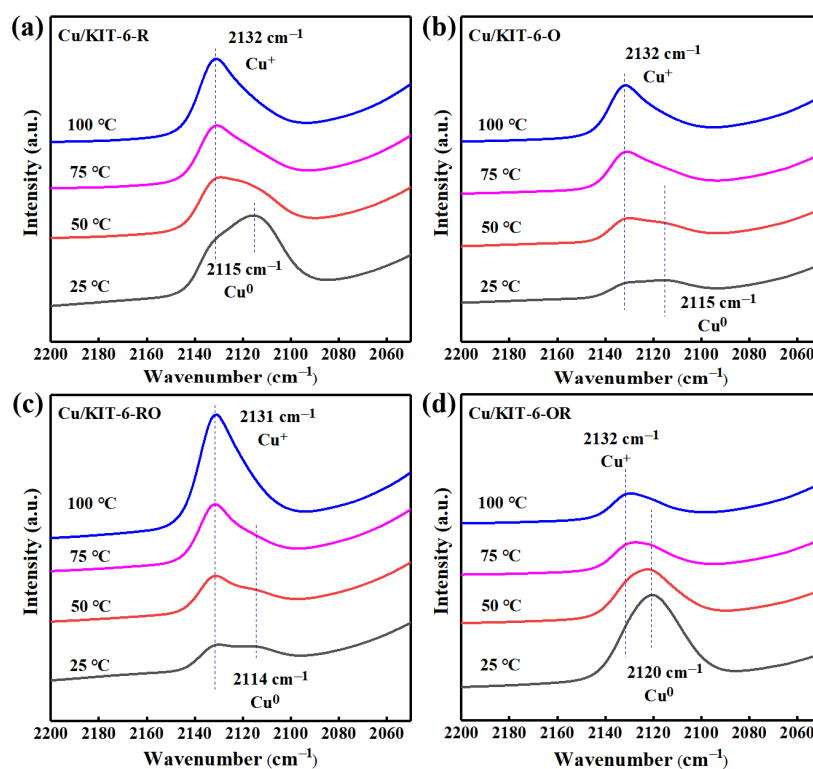


**Figure 8.** DRIFTS analysis of sequential adsorbed CO over the Cu/KIT-6 catalyst under different pre-treatment atmospheres: (a) R, (b) O, (c) RO, and (d) OR samples.

Additionally, copper valence not only affects the conversion of ethanol dehydrogenation, but also has a significant effect on the acetaldehyde selectivity. We speculated whether the treatment atmosphere also had an effect on acidity properties, and  $\text{NH}_3$ -TPD analysis was carried out by an in situ treatment of the catalyst, shown in Figure 7d. The peaks below 250 °C corresponded to the weak acid sites and the peaks at 250–400 °C were assigned to the moderate acid sites [40]. Both R and OR samples only showed an obvious weak acid peak, and the peak could be divided into two distinct  $\text{NH}_3$  desorption peak regions at ~105 °C and 130–170 °C, which were assigned to the adsorbed  $\text{NH}_3$  molecules at a weak acid site (surface hydroxyls, e.g., Si-OH). The weak acid amount for the R and OR samples were ~0.127 mmol/g and ~0.121 mmol/g, respectively. From the catalytic data, it can be seen that the acetaldehyde selectivity of the R and OR samples was similar at around 81%, which was attributed to no significant difference in the amount of weak acid between the two samples. Surprisingly, except for the weak acid peak, the RO sample exhibited a unique peak at ~286 °C, which represented the moderate acid sites related to the Cu species, perhaps due to the presence of  $\text{CuO}_x$  [41,42]. It has been reported that moderate acid sites are beneficial for ethanol dehydrogenation and enhance the selectivity to acetaldehyde [43], and the different quantity of moderate acid sites leads to the different total acidity of the catalysts, which possibly results in more active centers [38]. Therefore, the acetaldehyde selectivity of the RO sample (99.8%) was higher than that of R and OR. Moreover, the O sample also exhibited a similar peak at ~326 °C, attributed to the calcination of nitrate trihydrate to CuO [37,44], which confirmed that the moderate acid site was derived from CuO. The presence of a moderate acid site was the reason why the selectivity of the O sample for acetaldehyde (89.9%) was higher than R (81.4%) and OR (81.0%) at 250 °C. Therefore, the RO sample showed an excellent catalytic activity, which could be attributed to the moderate acid sites and suitable proportion of  $\text{Cu}^+/\text{Cu}^0$  ratio of ~0.53, which conceivably rendered its superior ethanol conversion of 96.8% and acetaldehyde selectivity of 99.8%.

## 2.4. Stability and Regeneration

We further explored the stability and recyclability of the Cu/KIT-6 catalyst by carrying out long time-on-stream experiments at 250 °C, and the results are presented in Figure 9a. After maintaining a conversion of 96.8% for about 20 h, the ethanol dehydrogenation reaction showed a decrease in the conversion of 0.54% per hour. The ethanol conversion remained at 74.5% after running for 96 h. Surprisingly, the acetaldehyde selectivity remained above 99% after 96 h. The deactivation mechanism of the catalyst was explored by performing some characterizations on the spent catalyst. Firstly, to determine whether there was a loss of Cu nanoparticles during the reaction, atomic absorption spectrometers were performed on the reacted catalysts. The comparative experiment revealed that no clear loss of Cu nanoparticles from the catalyst occurred, which indicated the good structural stability of this catalyst. Secondly, no significant growth of the Cu particles had taken place despite the extended time-on-stream. XRD patterns (Figure S5) exhibited no obvious diffraction peaks of Cu nanoparticles, indicating uniformly dispersed and small Cu crystallites. To further explore whether a loss of activity had been caused by the metal sintering mechanism, the TEM image of the spent catalysts showed that the average size of the Cu particles was ~2.10 nm, which remained unchanged compared with the fresh catalyst without aggregation (Figure S6). These results suggested that sintering was unlikely to be responsible for the decrease in catalytic activity. It was attributed to the fact that the nanoparticles exhibited a significant anti-aggregation ability even when heated to high temperatures due to the strong interfacial interaction between Cu and mesoporous silica, and the protective effect of ammonia water on Cu nanoparticles as a ligand [45]. Moreover, another important factor that was considered, was that fouling over the active sites may have led to deactivation of the catalyst. Therefore, the spent catalyst was reused under the same reaction conditions by heating in a flow of 20% O<sub>2</sub>/N<sub>2</sub> for 1 h at 250 °C, and surprisingly, almost recovered its high conversion (96.5%) and selectivity (99.5%). Additionally, this oxidative treatment successfully regenerated the catalyst to full activity even after three cycles. We speculated that fouling was the main cause of deactivation in our catalytic conditions. To further shed some light on the catalyst deactivation mechanism, the fresh catalyst, spent catalyst, and regenerated catalyst were characterized by in situ FTIR, as shown in Figure 9b.

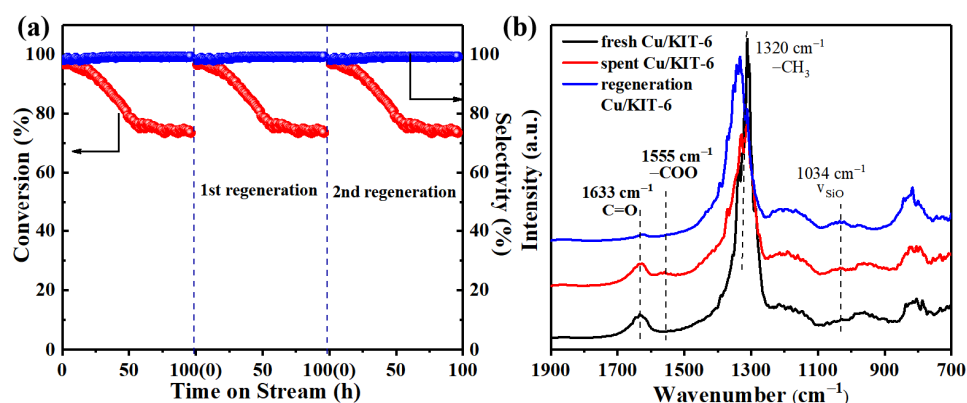


**Figure 9.** (a) Long time stability of the Cu/KIT-6 catalyst at 250 °C. Reaction condition: a reactant ethanol stream of 2 kPa balanced by N<sub>2</sub> under atmospheric pressure and WHSV of 13.67 mmol g<sup>-1</sup><sub>Cu</sub> h<sup>-1</sup>. Regeneration condition: oxidation at 250 °C for 1 h under 20% O<sub>2</sub>/N<sub>2</sub>. (b) In situ FTIR spectra of the fresh catalyst, spent catalyst, and regenerated catalyst.

The FTIR spectrum of the spent catalyst showed a small peak at approximately 1555 cm<sup>-1</sup> compared with the fresh catalyst, which was considered as a -COO group stretching vibrational absorption of acetic acid, and this peak disappeared after generation. According to the product analysis, the acetic acid content was very little, thus, we speculated that the formation of acetic acid was possibly due to the catalyst being exposed to air for a long time, which led to acetaldehyde oxidation to acetic acid [46]. Therefore, we

suspected that deactivation was attributable to the small amount of incompletely removed acetaldehyde that was adsorbed onto the active surface during the reaction, which blocked the active sites for the easy access of ethanol. The catalyst deactivation due to carbon deposits on the catalyst surface was easily removed by calcination, as active sites of the catalyst were “cleaned up” by removal of the strongly adsorbed organic species, and exposed to more  $\text{Cu}^+$  active centers [47]. In addition, the time-dependent in situ FTIR spectrum of the spent catalyst exposed to 10%  $\text{O}_2/\text{He}$  atmosphere at 250 °C for 1 h is shown in Figure S7. The -COO group stretching vibration intensity of acetic acid disappeared within only 1 min after exposure to an oxygen atmosphere, and there was almost no significant change with time, indicating that the organic species covering the catalyst surface was easily removed, which led to the activity recovery. The acetaldehyde selectivity remained unchanged due to the good stability of the catalyst. In summary, based on the fact that ammonia water acted as a ligand to protect Cu nanoparticles from agglomeration, it was observed that the prepared Cu/KIT-6 catalyst with a high metal dispersion could achieve excellent catalytic performance and a high selectivity to acetaldehyde, compared with the reported literature, as seen in Table 3.

**Table 3.** A comparative list of the reaction conditions and catalytic activities of ethanol dehydrogenation to acetaldehyde.

Catalysts	T (°C)	WHSV ( $\text{h}^{-1}$ )	$X_{\text{ethanol}}$ (%)	$S_{\text{acetaldehyde}}$ (%)	$Y_{\text{acetaldehyde}}$ (%)	Ref.
Cu/KIT-6	250	0.87	96.8	99.8	96.6	This work
Cu/SiO <sub>2</sub>	250	0.87	3.26	100	3.26	This work
Cu-MFI-AE <sup>a</sup>	250	0.53	97.9	93.1	91.1	[23]
Cu-MFI-IM <sup>b</sup>	250	0.53	64.4	89.4	57.6	[23]
Cu/MCM-41	300	-	90.0	90.0	81.0	[14]
Cu/SBA-15	300	2.1	72.0	37.0	27.0	[15]
Cu/SiO <sub>2</sub>	260	2.4	85.4	79.4	67.8	[48]
Cu/C/SiO <sub>2</sub>	260	2.4	83.0	95.1	78.9	[48]
Cu/ZnO	300	-	16.4	67.6	11.1	[10]
10Cu/ZrO <sub>2</sub>	275	3.2	81.5	13.6	11.1	[49]
Co@CN	400	18,000	66.0	84.0	55.4	[50]
ZnO-CuO-SiO <sub>2</sub>	400	3	92.8	72.7	67.5	[51]

<sup>a</sup> Cu-MFI-AE: the Cu-MFI was prepared by the ammonia evaporation method. <sup>b</sup> Cu-MFI-IM: the Cu-MFI was prepared by the incipient wetness impregnation method.

### 2.5. In Situ FTIR Studies

In situ FTIR study of ethanol adsorption was carried out over Cu/KIT-6 to further elucidate the structural influences on the surface adsorbates and intermediates, and the spectroscopy is shown in Figure 10. The band at  $\sim 3736 \text{ cm}^{-1}$  was the characteristic peak of isolated silanol groups. The bands of Si-OH had almost no change with temperature and time, which showed the dominance of isolated surface silanol groups. It can be clearly seen that the ethanol gas adsorbed on silica was converted into the adsorbed state on the surface of the catalysts with the increase in absorption time and temperature, which was located at  $\sim 1392 \text{ cm}^{-1}$ . The bands at  $\sim 3672 \text{ cm}^{-1}$ , with maximum intensity at room temperature, were assigned to the O-H stretching vibration of adsorbed ethanol on Cu species. The two dominant peaks were at 2984 and 2928  $\text{cm}^{-1}$ , which corresponded to the  $\text{CH}_3$  asymmetric and  $\text{CH}_2$  asymmetric stretching. These observations from the O-H and C-H stretching regimes suggested that adsorbed ethanol molecules were likely hydrogen bonded to the silica surface through silanol groups [2]. Figure 10a also shows that a new peak at  $\sim 2858 \text{ cm}^{-1}$  developed at 170 °C. This peak was assigned to the C-H stretching band of adsorbed ethoxy species ( $\text{CH}_2$  symmetric stretching). The ethanol was partially activated to form the Cu-ethoxy species based on the interactions between  $\text{Cu}^+$  and oxygen-containing species. In situ FTIR spectra indicated that silica support was active for the O-H bond scission of ethanol to form ethoxy species. The appearance of an

intense peak at  $\sim 1764\text{ cm}^{-1}$  was the characteristic peak of the C=O stretching vibration of acetaldehyde. More importantly, the decrease in ethoxy peaks and the increase in acetaldehyde peaks suggested that the formed ethoxy species underwent further C-H bond cleavage to acetaldehyde. In addition, ethylene (C=C) was produced as a side reaction by ethanol dehydration at higher reaction temperatures ( $>250\text{ }^{\circ}\text{C}$ ). Figure 10b exhibits the in situ FTIR spectra of the catalyst exposed to an ethanol atmosphere at  $250\text{ }^{\circ}\text{C}$  for different reaction times. The intensity of the C=O stretching vibration of acetaldehyde approached the steady state within only 1 min after exposure to the reaction atmosphere, indicating that the dehydrogenation of ethanol to acetaldehyde was a relatively rapid step. In fact, in situ FTIR results demonstrated that the C-H bond scission was the rate determining step in the reaction. The desorption of acetaldehyde on the catalyst surface was further explored, as shown in Figure 10c,d. The acetaldehyde peak gradually weakened with the increased temperatures, and the acetaldehyde peak had no obvious change under the acetaldehyde atmosphere for 120 min at  $250\text{ }^{\circ}\text{C}$ , demonstrating the good selectivity of ethanol to acetaldehyde over this catalyst.

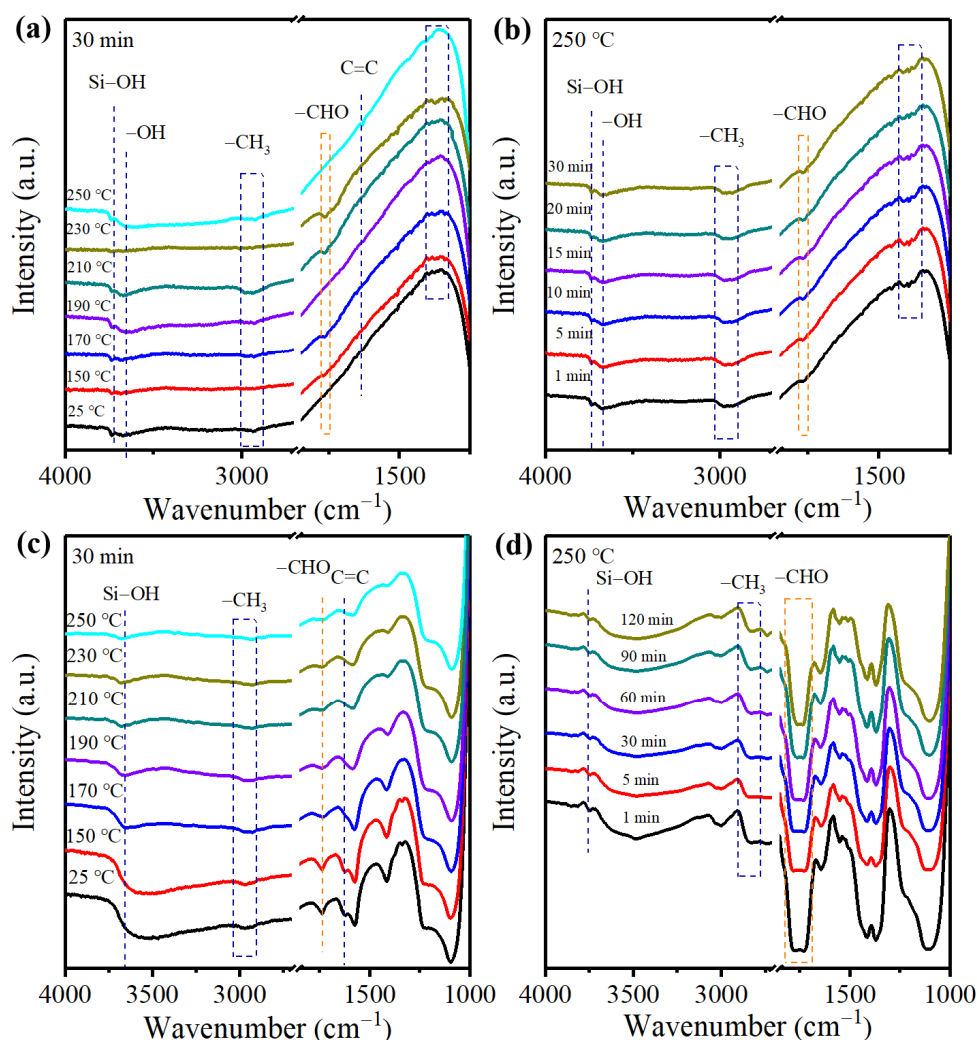


**Figure 10.** (a) In situ FTIR spectra of ethanol dehydration reaction over Cu/KIT-6 catalyst. The catalyst was exposed to ethanol atmosphere for 30 min at different temperatures followed by desorption. (b) In situ FTIR spectra of the catalyst exposed to ethanol atmosphere at  $250\text{ }^{\circ}\text{C}$  for different times. (c) In situ FTIR spectra of the catalyst exposed to acetaldehyde atmosphere for 30 min at different temperatures followed by desorption. (d) In situ FTIR spectra of the catalyst exposed to acetaldehyde atmosphere at  $250\text{ }^{\circ}\text{C}$  for different times.

Summarizing the results, the reaction pathway of ethanol dehydrogenation on silica-supported Cu catalysts is briefly described in Figure 11. Ethanol was preferably adsorbed on the active sites of catalysts, and  $\text{Cu}^+/\text{Cu}^0$  species were responsible for the ethanol adsorbed and activated in this reaction, which weakened the O-H bond and facilitated its cleavage. Afterward, the adsorbed ethanol was transformed to Cu(+)-ethoxy and H atoms, which were adsorbed on active sites. The C-H bond of Cu(+)-ethoxy was then activated by  $\text{Cu}^+$  to produce the adsorbed acetaldehyde, and then the acetaldehyde on  $\text{Cu}^+$  was desorbed to the gas phase [52]. The positive effect of the  $\text{Cu}^+/\text{Cu}^0$  species over the Cu/KIT-6 catalyst ensured the ethanol dehydrogenation reaction.

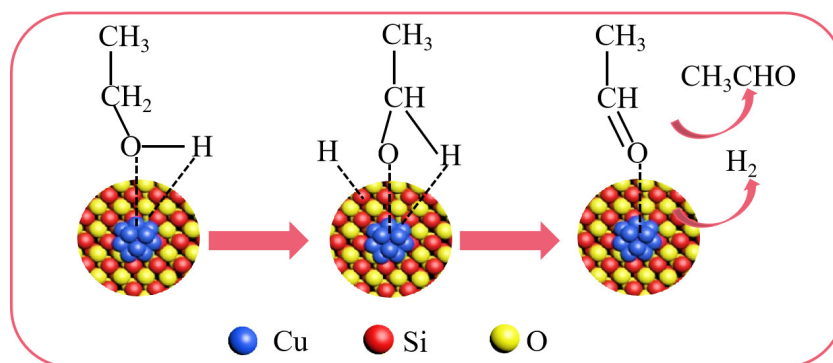


**Figure 11.** Possible reaction mechanism of ethanol dehydrogenation.

### 3. Materials and Methods

#### 3.1. Chemicals

Copper nitrate hydrate ( $\text{Cu}(\text{NO}_3)_2 \cdot 3\text{H}_2\text{O}$ ,  $\geq 99\%$ ), hydrochloric acid (HCl,  $\sim 37$  wt%), ethanol ( $\text{C}_2\text{H}_5\text{OH}$ ,  $\geq 99.7\%$ ), ammonia water ( $\text{NH}_3 \cdot \text{H}_2\text{O}$ , 25–28 wt%) and commercial silicon oxide ( $\text{SiO}_2$ ,  $\geq 95.8\%$ ) were purchased from Sinopharm Chemical Reagent Co. Ltd (Shanghai, China). Pluronic<sup>®</sup> P-123 was purchased from Sigma-Aldrich Co. (Shanghai, China). Tetraethyl orthosilicate (TEOS,  $\geq 99.99\%$ ) and dodecylamine (DDA,  $\geq 98.0\%$ ) were purchased from Shanghai Aladdin Biochemical Technology Co., Ltd. (Shanghai, China). *n*-Butanol ( $\text{BuOH}$ ,  $\geq 99.0\%$ ) was purchased from Tianjin Deen Chemical Reagent Co., Ltd. (Tianjin, China). All reagents were obtained from the supplier, without further purification.

#### 3.2. Catalyst Preparation

##### 3.2.1. Synthesis of Mesoporous Silica

The mesoporous SBA-15 [53], KIT-6 [54], and HMS [55] supports were prepared according to the reported literature, and the detailed synthesis steps are shown in Supplementary Materials Sections S2.1–S2.3.

##### 3.2.2. Cu Nanoparticles Supported on Various Silica Supports

The Cu/KIT-6 catalysts with different Cu loadings were tested in ethanol dehydrogenation, and the results are shown in Figure S8. The results showed that the Cu loading of  $\sim 10$  wt% exhibited the best catalytic activity. Therefore, the Cu theoretical loading of  $\sim 10$  wt% was selected to prepare Cu nanoparticles in this work, which has previously been reported as a suitable range of Cu loading to obtain enough active sites and avoid sintering deactivation [11]. The Cu nanoparticles were prepared by an electrostatic adsorption method and the detailed preparation procedures were as follows. Firstly, the mesoporous silica supports were dried at  $90^\circ\text{C}$  for 3 h prior to removal of water and impurities to the Cu precursor solution to load over the supports. Secondly, 0.42 g  $\text{Cu}(\text{NO}_3)_2 \cdot 3\text{H}_2\text{O}$  was added to 34 mL ammonia water to obtain a copper ammonium solution. Then, 437 mL of deionized water was added, and the pH adjusted to about 11.5 by ammonia water, and sealed with plastic wrap. Subsequently, 1.0 g support was added and stirred for 10 min at room temperature with a rotation speed of 600 rpm. The samples were suction filtered,

washed, dried at 50 °C overnight, and further calcined in an air muffle furnace at 120 °C for 4 h. Finally, the samples were reduced at 350 °C (10% H<sub>2</sub>/Ar) for 1 h, cooled to room temperature and purged with N<sub>2</sub> for 1 h, and then oxidized at 350 °C (20% O<sub>2</sub>/N<sub>2</sub>) for 1 h to obtain 7.80 wt% Cu/KIT-6, 7.16 wt% Cu/SBA-15, and 7.75 wt% Cu/HMS composite. The Cu content of the sample was determined by an atomic absorption spectrometer. In addition, the Cu/KIT-6-none catalyst was prepared under the same preparation and processing conditions, except without the addition of ammonia water. The Cu/SiO<sub>2</sub> catalyst was prepared by the commercial silica support under the same preparation and processing conditions.

### 3.2.3. Cu/KIT-6 Catalyst Treated under Various Atmospheres

The Cu/KIT-6 catalyst prepared by the above method was used to study the effect of treatment atmosphere on the catalytic performances of the ethanol dehydrogenation reaction, and the treatment temperature was kept at 350 °C. The catalyst reduced under 10% H<sub>2</sub>/Ar for 1 h was named as R, and the catalyst oxidized under 20% O<sub>2</sub>/N<sub>2</sub> for 1 h was named as O. The catalyst reduced under 10% H<sub>2</sub>/Ar for 1 h, cooled to room temperature and purged with N<sub>2</sub> for 1 h, and then oxidized under 20% O<sub>2</sub>/N<sub>2</sub> for 1 h, was named as RO. The catalyst oxidized under 20% O<sub>2</sub>/N<sub>2</sub> for 1 h, cooled to room temperature and purged with N<sub>2</sub> for 1 h, and then reduced under 10% H<sub>2</sub>/Ar for 1 h, was named as OR.

### 3.3. Catalyst Characterization

The catalyst characterization techniques are described in the Supplementary Materials Sections S3.1–S3.6.

### 3.4. Catalytic Activity

Catalyst performance test of ethanol dehydrogenation was carried out in a fixed bed reactor under atmospheric pressure. The catalyst was placed in a quartz tube (8 mm × 380 mm). Ethanol was fed to the system via a vaporizer, producing a reactant stream composed of ethanol (2 kPa) balanced by an N<sub>2</sub> flow of 36 mL/min under atmospheric pressure, and WHSV (weight hourly space velocity) was 13.67 mmol g<sup>-1</sup>Cu h<sup>-1</sup>, which was calculated by Equation (1). The Cu amount of the sample, determined by an atomic absorption spectrometer, was measured by the average value of the obtained data based on the standard curve. The reaction products were analyzed by gas chromatography (GC-9160 chromatograph) equipped with a FID detector and PONA capillary column (50 m × 0.20 mm × 0.5 μm), in which 2-propanol was employed as the internal standard [56]. The ethanol conversion ( $X_{EtOH}$ ), acetaldehyde selectivity ( $S_{AcH}$ ), acetaldehyde yield ( $Y$ ) and normalized reaction rate ( $r$ ) for ethanol conversion were calculated using Equations (2)–(5), respectively.

$$WHSV = \frac{m_{EtOH}/hour}{m_{Cu}} \quad (1)$$

$$X_{EtOH} = \frac{EtOH_{in} - EtOH_{out}}{EtOH_{in}} \times 100\% \quad (2)$$

$$S_{AcH} = \frac{AcH}{EtOH_{in} - EtOH_{out}} \times 100\% \quad (3)$$

$$Y_{AcH} = X_{EtOH} \times S_{AcH} / 100 \quad (4)$$

$$r_{Ethanol} = \frac{M_{Cu} \times X_{EtOH} \times F_{EtOH}}{m_{cat} \times \%Cu \times D_{Cu} / 100} \quad (5)$$

where  $F_{EtOH}$  was the ethanol molar flow in the reactor inlet (mol s<sup>-1</sup>);  $X_{EtOH}$  was the ethanol conversion (%);  $m_{cat}$  was the catalyst weight (g);  $m_{Cu}$  was the active metal weight (g);  $m_{EtOH}$  was the reactant ethanol weight (g);  $\%Cu$  was the copper loading (%),  $M_{Cu}$  was copper molar weight (63.55 g mol<sup>-1</sup>), and  $D_{Cu}$  was the copper dispersion obtained by N<sub>2</sub>O titration method (%).

#### 4. Conclusions

The Cu/KIT-6 catalyst showed a higher catalytic behavior than Cu/SBA-15 and Cu/HMS catalysts at 250 °C, due to the three-dimensional pore structure, uniformly distributed Cu nanoparticles, higher active surface area and metal dispersion, and the abundant acid sites, which enabled the Cu/KIT-6 catalyst to behave as the best candidate in ethanol dehydrogenation. Moreover, the treatment atmosphere of the catalyst affected both the valence state of the copper species and the acidity properties. The existence of an oxidation atmosphere had a significant effect on the valence state of the copper species and in enhancing moderate acid sites. The catalyst treated by reduction and then oxidation possessed abundant moderate acid sites and a suitable proportion of Cu<sup>+</sup>/Cu<sup>0</sup> ratio of ~0.53. In situ FTIR results showed that the C-H bond scission was the rate determining step during the reaction, and the acetaldehyde peak had no obvious change under the acetaldehyde atmosphere for 120 min at 250 °C, demonstrating the good selectivity of ethanol to acetaldehyde. Hence, Cu/KIT-6 catalyst prepared by the electrostatic adsorption method can be used as an alternative method to develop a highly dispersed nanocatalyst to improve catalytic efficiency.

**Supplementary Materials:** The following supporting information can be downloaded at: <https://www.mdpi.com/article/10.3390/catal12091049/s1>, Figure S1: The XRD spectra of HMS and Cu/HMS catalysts; Figure S2: XPS spectra of (a) Cu/KIT-6, (b) Cu/SBA-15, and (c) Cu/HMS, catalysts; Figure S3: (a) TEM image of Cu/KIT-6-none, (b) ethanol conversion and product selectivity of the Cu/KIT-6-none; reaction condition: a reactant ethanol stream of 2 kPa balanced by N<sub>2</sub> under atmospheric pressure and WHSV of 13.67 mmol g<sup>-1</sup><sub>Cu</sub> h<sup>-1</sup>; Figure S4: H<sub>2</sub>-TPR analysis of the CuO sample; Figure S5: XRD pattern of the spent Cu/KIT-6 catalyst after running for 96 h; Figure S6: TEM image of the spent Cu/KIT-6 catalyst after running for 96 h; Figure S7: In situ FTIR spectra of the spent Cu/KIT-6 catalyst exposed to 10% O<sub>2</sub>/He atmosphere at 250 °C for 1 h; Figure S8: (a) ethanol conversion and (b) acetaldehyde selectivity and yield of the Cu/KIT-6 catalysts with different Cu loading; reaction condition: a reactant ethanol stream of 2 kPa balanced by N<sub>2</sub> under atmospheric pressure and WHSV of 13.67 mmol g<sup>-1</sup><sub>Cu</sub> h<sup>-1</sup>.

**Author Contributions:** Conceptualization, Y.H.; methodology, Y.H. and D.Z.; validation, D.Z., W.L., M.Z. and Y.L.; investigation, Z.W.; writing—original draft preparation, Y.H.; writing—review and editing, Q.T. and J.Y.; supervision, Q.T. and J.Y.; funding acquisition, Y.H. and J.Y. All authors have read and agreed to the published version of the manuscript.

**Funding:** This work was supported by the National Natural Science Foundation of China (Nos. 21701103 and 21671122), Natural Science Foundation of Henan province (162300410175), Key Scientific Research Project of Colleges and Universities in Henan (22A150044).

**Data Availability Statement:** The results in this work were not previously published anywhere.

**Acknowledgments:** The authors thank the Centre for Instrumental Analysis, School of Chemistry and Chemical Engineering, Henan Normal University for analysis support in this project.

**Conflicts of Interest:** The authors declare no conflict of interest.

#### References

1. Ob-eye, J.; Prasertthadam, P.; Jongsomjit, B. Dehydrogenation of ethanol to acetaldehyde over different metals supported on carbon catalysts. *Catalysts* **2019**, *9*, 66. [[CrossRef](#)]
2. Shan, J.; Liu, J.; Li, M.W.; Lustig, S.; Stephanopoulos, M.F. NiCu single atom alloys catalyze the C-H bond activation in the selective non-oxidative ethanol dehydrogenation reaction. *Appl. Catal. B Environ.* **2018**, *226*, 534–543. [[CrossRef](#)]
3. Chen, A.; Yu, X.; Zhou, Y.; Sehested, J.; Wang, Y.; Shen, W. Structure of the catalytically active copper-ceria interfacial perimeter. *Nat. Catal.* **2019**, *2*, 334–341. [[CrossRef](#)]
4. Rosset, M.; Perez-Lopez, O.W. Cu-Ca-Al catalysts derived from hydrocalumite and their application to ethanol dehydrogenation. *React. Kinet. Mech. Catal.* **2019**, *126*, 497–511. [[CrossRef](#)]
5. Huang, Y.J.; Wang, B.; Yuan, H.K.; Sun, Y.B.; Yang, D.Y.; Cui, X.J.; Shi, F. The catalytic dehydrogenation of ethanol by heterogeneous catalysts. *Catal. Sci. Technol.* **2021**, *11*, 1652–1664. [[CrossRef](#)]
6. Sato, A.G.; Volanti, D.P.; Meira, D.M.; Damyanova, S.; Longo, E.; Bueno, J.M.C. Effect of the ZrO<sub>2</sub> phase on the structure and behavior of supported Cu catalysts for ethanol conversion. *J. Catal.* **2013**, *307*, 1–17. [[CrossRef](#)]

7. Shiao, C.Y.; Lee, Y.R. Characterization and dehydrogenation activity of Cr-added electroless plated copper catalyst. *Appl. Catal. A Gen.* **2001**, *220*, 173–180. [[CrossRef](#)]
8. Hanukovich, S.; Dang, A.; Christopher, P. Influence of metal oxide support acid sites on Cu-catalyzed nonoxidative dehydrogenation of ethanol to acetaldehyde. *ACS Catal.* **2019**, *9*, 3537–3550. [[CrossRef](#)]
9. Fujita, S.; Iwasa, N.; Tani, H.; Nomura, W.; Arai, M.; Takezawa, N. Dehydrogenation of ethanol over Cu/ZnO catalysts prepared from various coprecipitated precursors. *React. Kinet. Catal. Lett.* **2001**, *73*, 367–372. [[CrossRef](#)]
10. Gao, D.; Feng, Y.H.; Yin, H.B.; Wang, A.; Jiang, T.S. Coupling reaction between ethanol dehydrogenation and maleic anhydride hydrogenation catalyzed by Cu/Al<sub>2</sub>O<sub>3</sub>, Cu/ZrO<sub>2</sub>, and Cu/ZnO catalysts. *Chem. Eng. J.* **2013**, *233*, 349–359. [[CrossRef](#)]
11. Phung, T.K. Copper-based catalysts for ethanol dehydrogenation and dehydrogenative coupling into hydrogen, acetaldehyde and ethyl acetate. *Int. J. Hydrogen Energy* **2021**, *11*, 253–268. [[CrossRef](#)]
12. Wang, N.; Yu, X.; Shen, K.; Chu, W.; Qian, W. Synthesis, characterization and catalytic performance of MgO-coated Ni/SBA-15 catalysts for methane dry reforming to syngas and hydrogen. *Int. J. Hydrogen Energy* **2013**, *38*, 9718–9731. [[CrossRef](#)]
13. Zhou, G.L.; Zhang, H.B.; Xie, H.M.; Wu, M.; Wei, M.Y. Ethanol catalytic oxidation on ordered mesoporous CuO/KIT-6 catalyst. *Int. J. Chem. React. Eng.* **2013**, *11*, 259–263. [[CrossRef](#)]
14. Finger, P.H.; Osmari, T.A.; Cabral, N.M.; Bueno, J.C.; Gallo, J.M.R. Direct synthesis of Cu supported on mesoporous silica: Tailoring the Cu loading and the activity for ethanol dehydrogenation. *Catal. Today* **2021**, *381*, 26–33. [[CrossRef](#)]
15. Gao, D.Z.; Wang, A.; Shen, L.Q.; Liu, S.X. Gas phase dehydrogenation of ethanol using maleic anhydride as hydrogen acceptor over Cu/hydroxylapatite, Cu/SBA-15, and Cu/MCM-41 catalysts. *J. Ind. Eng. Chem.* **2015**, *26*, 322–332. [[CrossRef](#)]
16. Feng, Z.L.; Bai, X.F. 3D-mesoporous KIT-6 supported highly dispersed Pd nanocatalyst for dodecahydro-*N*-ethylcarbazole dehydrogenation. *Micropor. Mesopor. Mat.* **2022**, *335*, 111789–111800. [[CrossRef](#)]
17. Zaccheria, F.; Scotti, N.; Marelli, M.; Psaro, R.; Ravasio, N. Unravelling the properties of supported copper oxide: Can the particle size induce acidic behaviour? *Dalton Trans.* **2013**, *42*, 1319–1328. [[CrossRef](#)]
18. Wong, A.; Liu, Q.; Griffin, S.; Nicholls, A.; Regalbuto, J.R. Synthesis of ultrasmall, homogeneously alloyed, bimetallic nanoparticles on silica supports. *Science* **2017**, *358*, 1427–1430. [[CrossRef](#)]
19. Zhang, H.W.; Tan, H.R.; Jaenicke, S.; Chuah, G.K. Highly efficient and robust Cu catalyst for non-oxidative dehydrogenation of ethanol to acetaldehyde and hydrogen. *J. Catal.* **2020**, *389*, 9–28. [[CrossRef](#)]
20. Subhan, F.; Aslam, S.; Yan, Z.; Ikram, M.; Rehman, S. Enhanced desulfurization characteristics of Cu-KIT-6 for thiophene. *Micropor. Mesopor. Mat.* **2014**, *199*, 108–116. [[CrossRef](#)]
21. Miao, K.K.; Luo, X.L.; Guo, J.L.; Cao, F.J.; Hu, Y.Q.; Feng, G.D. One-step synthesis of Cu-SBA-15 under neutral condition and its oxidation catalytic performance. *Micropor. Mesopor. Mat.* **2019**, *289*, 109640–109648. [[CrossRef](#)]
22. Fu, Z.H.; Chen, J.H.; Yin, D.L.; Yin, D.H.; Zhang, L.X.; Zhang, Y.Y. Highly effective Cu-HMS catalyst for hydroxylation of phenol. *Catal. Lett.* **2000**, *66*, 105–108. [[CrossRef](#)]
23. Pang, J.F.; Zheng, M.Y.; Yang, X.F.; Wang, Y.; Zhang, T. Hierarchical echinus-like Cu-MFI catalysts for ethanol dehydrogenation. *ACS Catal.* **2020**, *10*, 13624–13629. [[CrossRef](#)]
24. Kim, D.; Becknell, N.; Yu, Y.; Yang, P. Room-temperature dynamics of vanishing copper nanoparticles supported on silica. *Nano Lett.* **2017**, *17*, 2732–2737. [[CrossRef](#)]
25. Wang, J.; Huang, Y.; Yu, T.; Zhu, S.C.; Shen, M.Q.; Li, W.; Wang, J.Q. The migration of Cu species over Cu-SAPO-34 and its effect on NH<sub>3</sub> oxidation at high temperature. *Catal. Sci. Technol.* **2014**, *4*, 3004–3012. [[CrossRef](#)]
26. Cassinelli, W.H.; Martins, L.; Passos, A.R.; Pulcinelli, S.H.; Rochet, A.; Briois, V.; Santilli, C.V. Correlation between structural and catalytic properties of copper supported on porous alumina for the ethanol dehydrogenation reaction. *ChemCatChem* **2015**, *7*, 1668–1677. [[CrossRef](#)]
27. Reddy, K.P.; Choi, H.; Kim, D.; Ryoo, R.; Park, J.Y. Cu oxide deposited on shape-controlled ceria nanocrystals for CO oxidation: Influence of interface-driven oxidation states on catalytic activity. *Catal. Sci. Technol.* **2021**, *11*, 6134–6142. [[CrossRef](#)]
28. He, Z.; Lin, H.Q.; He, P.; Yuan, Y.Z. Effect of boric oxide doping on the stability and activity of a Cu-SiO<sub>2</sub> catalyst for vapor-phase hydrogenation of dimethyl oxalate to ethylene glycol. *J. Catal.* **2011**, *277*, 54–63. [[CrossRef](#)]
29. Amokrane, S.; Boualouache, A.; Simon, P.; Capron, M.; Otmanine, G.; Allam, D.; Hocine, S. Effect of adding transition metals to copper on the dehydrogenation reaction of ethanol. *Catal. Lett.* **2021**, *151*, 2864–2883. [[CrossRef](#)]
30. Li, M.Y.; Lu, W.D.; He, L.; Schüth, F.; Lu, A.H. Tailoring the surface structure of silicon carbide support for copper catalyzed ethanol dehydrogenation. *ChemCatChem* **2019**, *11*, 481–487. [[CrossRef](#)]
31. Patel, A.; Shukla, P.; Rufford, T.; Wang, S.; Chen, J.; Rudolph, V.; Zhu, Z. Catalytic reduction of NO by CO over copper-oxide supported mesoporous silica. *Appl. Catal. A Gen.* **2011**, *409–410*, 55–65. [[CrossRef](#)]
32. Li, L.D.; Guan, N.J. HC-SCR reaction pathways on ion exchanged ZSM-5 catalysts. *Micropor. Mesopor. Mat.* **2009**, *117*, 450–457. [[CrossRef](#)]
33. Ming, S.; Wang, P.; Liu, P.; Duan, J.H.; Mei, F.M.; Pang, L.; Chen, Z.; Li, T. Promotional effect of metal cations doping on OMS-2 catalysts for NH<sub>3</sub>-SCR Reaction. *Chem. Eng. J.* **2020**, *379*, 122287–122297. [[CrossRef](#)]
34. Gao, J.S.; Han, Y.L.; Mu, J.C.; Wu, S.C.; Tan, F.; Shi, Y.; Li, X.Y. 2D, 3D mesostructured silicas templated mesoporous manganese dioxide for selective catalytic reduction of NO<sub>x</sub> with NH<sub>3</sub>. *J. Colloid Interf. Sci.* **2018**, *516*, 254–262. [[CrossRef](#)]
35. Sridevi, B.; Nagaiah, P.; Padmasri, A.H.; Raju, B.D.; Rao, K.S.R. Studies on dehydrogenation of cyclohexanol to cyclohexanone over mesoporous SiO<sub>2</sub> supported copper catalysts. *J. Chem. Sci.* **2017**, *129*, 601–608. [[CrossRef](#)]

36. Ding, T.; Tian, H.; Liu, J.; Wu, W.; Yu, J. Highly active Cu/SiO<sub>2</sub> catalysts for hydrogenation of diethyl malonate to 1,3-propanediol. *Chin. J. Catal.* **2016**, *37*, 484–493. [[CrossRef](#)]
37. Marino, F.J.; Cerrella, E.G.; Duhalde, S.; Jobbagy, M.; Laborde, M.A. Hydrogen from steam reforming of ethanol. characterization and performance of copper-nickel supported catalysts. *Int. J. Hydrogen Energy* **1998**, *23*, 1095–1101. [[CrossRef](#)]
38. Li, F.J.; Wang, L.G.; Han, X.; Cao, Y.; He, P.H.; Li, Q. Selective hydrogenation of ethylene carbonate to methanol and ethylene glycol over Cu/SiO<sub>2</sub> catalysts prepared by ammonia evaporation method. *Int. J. Hydrogen Energy* **2017**, *42*, 2144–2156. [[CrossRef](#)]
39. Campisano, I.S.P.; Rodella, C.B.; Sousa, Z.S.B.; Henriques, C.A.; Silva, V.T. Influence of thermal treatment conditions on the characteristics of Cu-based metal oxides derived from hydrotalcite-like compounds and their performance in bio-ethanol dehydrogenation to acetaldehyde. *Catal. Today* **2018**, *306*, 111–120. [[CrossRef](#)]
40. Zhu, S.; Gao, X.; Zhu, Y.; Zheng, H.; Li, Y. Promoting effect of boron oxide on Cu/SiO<sub>2</sub> catalyst for glycerol hydrogenolysis to 1,2-propanediol. *J. Catal.* **2013**, *303*, 70–79. [[CrossRef](#)]
41. Albert, K.B.; Fan, C.; Pang, L.; Chen, Z.; Ming, S.J.; Albert, T.; Li, T. The influence of chemical poisoning, hydrothermal aging and their coeffects on Cu-SAPO-34 catalyst for NO<sub>x</sub> reduction by NH<sub>3</sub>-SCR. *Appl. Surf. Sci.* **2019**, *479*, 1200–1211. [[CrossRef](#)]
42. Zhang, T.; Shi, J.; Liu, J.; Wang, D.; Zhao, Z.; Cheng, K.; Li, J. Enhanced hydrothermal stability of Cu-ZSM-5 catalyst via surface modification in the selective catalytic reduction of NO with NH<sub>3</sub>. *Appl. Surf. Sci.* **2016**, *375*, 186–195. [[CrossRef](#)]
43. Manriquez, M.E.; Lopez, T.; Gomez, R.; Navarrete, J. Preparation of TiO<sub>2</sub>-ZrO<sub>2</sub> mixed oxides with controlled acid-basic properties. *J. Mol. Catal. A Gen.* **2004**, *220*, 229–237. [[CrossRef](#)]
44. van der Grift, C.J.G.; Wielers, A.F.H.; Mulder, A.; Geus, J.W. The reduction behaviour of silica-supported copper catalysts prepared by deposition-precipitation. *Thermochim. Acta* **1990**, *171*, 95–113. [[CrossRef](#)]
45. Heemeier, M.; Stempel, S.; Shaikhutdinov, S.K.; Libuda, J.; Bäumer, M.; Oldman, R.J.; Jackson, S.D.; Freund, H.J. On the thermal stability of metal particles supported on a thin alumina film. *Surf. Sci.* **2003**, *523*, 103–110. [[CrossRef](#)]
46. Raskó, J.; Kiss, J. Adsorption and surface reactions of acetaldehyde on TiO<sub>2</sub>, CeO<sub>2</sub> and Al<sub>2</sub>O<sub>3</sub>. *Appl. Catal. A Gen.* **2005**, *287*, 252–260. [[CrossRef](#)]
47. Hao, Y.; Hao, G.P.; Guo, D.C.; Lu, A.H. Bimetallic Au–Pd nanoparticles confined in tubular mesoporous carbon as highly selective and reusable benzyl alcohol oxidation catalysts. *ChemCatChem* **2012**, *4*, 1595–1602. [[CrossRef](#)]
48. Wang, Q.N.; Shi, L.; Li, W.; Li, W.C.; Si, R.F.; Lu, A.H. Cu supported on thin carbon layer-coated porous SiO<sub>2</sub> for efficient ethanol dehydrogenation. *Catal. Sci. Technol.* **2018**, *8*, 472–479. [[CrossRef](#)]
49. Freitas, I.C.; Damyanova, S.; Oliveira, D.C.; Marques, C.M.P.; Bueno, J.M.C. Effect of Cu content on the surface and catalytic properties of Cu/ZrO<sub>2</sub> catalyst for ethanol dehydrogenation. *J. Mol. Catal. A Chem.* **2014**, *381*, 26–37. [[CrossRef](#)]
50. Chernov, A.N.; Astrakova, T.V.; Koltunov, K.Y.; Sobolev, V.I. Ethanol dehydrogenation to acetaldehyde over Co@N-Doped carbon. *Catalysts* **2021**, *11*, 1411. [[CrossRef](#)]
51. Kustov, A.L.; Tarasov, A.L.; Tkachenko, O.P.; Mishin, I.V.; Kapustin, G.I.; Kustov, L.M. Ethanol to acetaldehyde conversion under thermal and microwave heating of ZnO-CuO-SiO<sub>2</sub> modified with WC nanoparticles. *Molecules* **2021**, *26*, 1955. [[CrossRef](#)]
52. Wang, Z.T.; Hoyt, R.A.; El-Soda, M.; Madix, R.J.; Kaxiras, E.; Sykes, E.C.H. Dry dehydrogenation of ethanol on Pt-Cu single atom alloys. *Top. Catal.* **2018**, *61*, 328–335. [[CrossRef](#)]
53. Akti, F.; Balci, S.; Dogu, T. Role of synthesis media on properties of tin and copper incorporated SBA-15 catalysts and their activity in selective oxidation of ethanol. *Mater. Chem. Phys.* **2019**, *223*, 249–259. [[CrossRef](#)]
54. He, F.; Luo, J.Q.; Liu, S.T. Novel metal loaded KIT-6 catalysts and their applications in the catalytic combustion of chlorobenzene. *Chem. Eng. J.* **2016**, *294*, 362–370. [[CrossRef](#)]
55. Pauly, T.R.; Pinnavaia, T.J. Pore size modification of mesoporous HMS molecular sieve silicas with wormhole framework structures. *Chem. Mater.* **2001**, *13*, 987–993. [[CrossRef](#)]
56. Ai, P.P.; Tan, M.H.; Yamane, N.; Liu, G.G.; Fan, R.G.; Yang, G.H.; Yoneyama, Y.; Yang, R.Q.; Tsubaki, N. Synergistic effect of a boron-doped carbon-nanotube-supported Cu catalyst for selective hydrogenation of dimethyl oxalate to ethanol. *Chem. Eur. J.* **2017**, *23*, 8252–8261. [[CrossRef](#)]